ELSEVIER

Physica D 76 (1994) 123–146

PHYSICA D

Tracer dynamics in open hydrodynamical flows as chaotic scattering

E.M. Ziemniak [a], C. Jung [b], T. Tél [c]

[a] *Ruhr-Universität Bochum, D-44801 Bochum, Germany*

[b] *Fachbereich Physik, Universität Bremen, D-28359 Bremen, Germany*

[c] *Institute for Theoretical Physics, Eötvös University, H-1088 Budapest, Puskin u. 5–7, Hungary*

Abstract

Methods coming from the theory of chaotic scattering are applied to the advection of passive particles in an open hydrodynamical flow. In a region of parameters where a von Kármán vortex street is present with a time periodic velocity field behind a cylinder in a channel, particles can temporarily be trapped in the wake. They exhibit chaotic motion there due to the presence of a nonattracting chaotic set. The experimentally well-known concept of streaklines is interpreted as a structure visualising asymptotically the unstable manifold of the full chaotic set. The evaluation of streaklines can also provide characteristic numbers of this invariant set, e.g. topological entropy, Lyapunov exponent, escape rate. The time delay distributions are also evaluated. We demonstrate these ideas with the aid of both computer simulations of the Navier-Stokes equations and analytical model computations. Properties that could be measured in a laboratory experiment are discussed.

1. Introduction

The passive advection of particles in hydrodynamical systems has attracted recent interest in both closed [1–14] and open flows [15–29], and lead to a mutual interaction between the fields of fluid dynamics and dynamical systems. Passive advection has widespread applications in nature as, e.g., transport of pollution in fluids, aerosols, solidified particles in melts and magmas, etc. It is also important for the mixing of particles in flows.

Theoretical investigations have mainly concentrated on two-dimensional incompressible flows where the existence of a streamfunction $\psi(x,y,t)$ is maintained. Since the velocity components are obtained as spatial derivatives of ψ, the equations of motion of a particle advected by the flow are

$$\frac{d}{dt}x(t) = \frac{\partial}{\partial y}\psi(x,y,t), \tag{1}$$

$$\frac{d}{dt}y(t) = -\frac{\partial}{\partial x}\psi(x,y,t). \tag{2}$$

The key observation is that these equations have exactly the same structure as the canonical equations of motion for a particle moving along a 1-dimensional position space without any friction under the influence of an explicitly time-dependent force. The following identifications can be made: $x \to q$ where q is the position of the particle, $y \to p$ where p is the canonically conjugate momentum of the particle, $\psi(x,y,t) \to$

0167-2789/94/$07.00
SSDI 0167-2789(94)00045-R

$H(q,p,t)$ where H is the Hamiltonian of the dynamics. It is well known that driven Hamiltonian systems with one degree of freedom can exhibit chaotic behaviour of essentially the same type as autonomous systems with 2 degrees of freedom. Therefore, the particle transport is typically chaotic in time-dependent flows.

An especially appealing property of this phenomenon is that the phase space of the particle dynamics *coincides* with the configuration space. The phase space structures thus become observable by the naked eye. Since the Lagrangian equations of motion (1),(2) are independent of whether the flow is ideal or viscous, in the latter case laboratory experiments can be designed for the investigation of the tracer dynamics. For closed flows a series of experiments has already been carried out [3,4,9] and provided complete agreement with the results of dynamical systems' theory.

In this paper we concentrate on *open* flows around obstacles and show that the passive advection in such cases is equally well suited for experimental investigations as in closed geometries. The nonstationarity of the flow is often restricted to a finite region around the obstacle(s), outside of which the velocity field is practically stationary. In this asymptotic region the stream function is time-independent and the Lagrangian dynamics is integrable. The openness of the system and the asymptotic simplicity of the motion makes then advection analogous to particle *scattering*. Nevertheless, particles may exhibit complicated motion in the vicinity of the obstacle(s), in the region in which the velocity field is strongly time-dependent. The behaviour is typically chaotic here and the motion of particles is then a realization of *chaotic scattering* [24,27,29–33]. With modern techniques it seems to be possible to investigate particle trajectories in detail [15,17,69,71] and we think that the experimental investigation of passive particles in open flows behind obstacles might be the first detailed observation of classical chaotic scattering in an experiment.

Based on numerical simulation, we give a qualitative description of the most important phenomena connected with the passive transport process and summarize those quantities which could be measured in laboratory experiments.

For demonstration we choose the von Kármán vortex street since it is one of the well known examples of coherent flow patterns, which has a parameter interval leading to a time periodic velocity field. For this system there exists a lot of experimental data [16,34–38,57] and it also has various important applications.

It is well known that the solution to the Euler problem, i.e., the velocity field of the Navier-Stokes equations can also be more complicated than periodic. In some cases chaotic behaviour has been observed (see e.g. [39]), while for large Reynolds numbers turbulence sets in (see e.g. [40] in an experiment and [41,42] in computer simulations). It was even possible to do analytical investigations leading to a description in terms of stochastic processes (see e.g. [43]).

We are interested to establish a connection of the advection problem to Hamiltonian dynamics which is clearly possible for 2-dimensional periodic flows. Therefore, we restrict our considerations to the case of small Reynolds numbers where it is well established that the flow is essentially 2-dimensional [34,38]. For our line of argumentation it is useful that the 2-dimensional position space of the flow coincides with the 2-dimensional phase space of the related Hamiltonian system. To maintain this coincidence, it is neccessary to restrict the kinematics to passive advection of point particles. It would break down, howewer, if we allow for more general types of advection (extended particles, particles with excess inertia) which have already been treated in various investigations [25,44–46].

The passive advection in the wake of a cylinder has also been investigated recently by Shariff, Pulliam, and Ottino [22]. They treated the problem of a compressible fluid and concentrated on the determination of the invariant manifolds of

some singular points on the cylinder's surface and of a period-one orbit in the wake. These authors showed that the material lines of dye particles (streaklines) converge to the unstable manifold emanating from the singular points on the surface.

Our investigation is based on the *analogy* between the Lagrangian dynamics and chaotic scattering. Because the assumed incompressiblity of the flow implies the Hamiltonian character of the particle dynamics, methods of classical scattering theory become applicable. We study particle trajectories, periodic orbits, invariant manifolds, the chaotic set, time delay functions and time delay statistics. These investigations also enable us to *quantitatively* characterize chaos by computing the escape rate, topological entropy, Lyapunov exponents and the fractal dimension of the chaotic set.

The paper is organized as follows. In Section 2 we briefly summarize what chaotic scattering is. Next, the Eulerian problem studied in this paper is described, the flow behind a cylinder in a channel at Reynolds number where the velocity field is periodic and a von Kármán vortex street is present. (An analytical model flow used to obtain high resolution results, as a complementary fit to the solution of the direct numerical simulation of the Navier-Stokes equations, is presented in the Appendix.) The remaining part of the paper is devoted to the Lagrangian problem, to the passive advection of particles in this time-periodic velocity field. Section 4 discusses the form of particle trajectories, as well as certain basic periodic orbits acting as a building block for an infinity of other periodic orbits present in the problem. It is also shown that periodic orbits can be shifted close to the surface of the cylinder with increasing period. This will be the source of an algebraic long time behaviour observed in the time delays. The chaotic invariant set with fractal properties in which all of these periodic orbits are embedded is treated in the Section 5, along with its invariant manifolds. We point out that those segments of the streaklines that remain in the wake of the cylinder converge to the unstable manifold of the full chaotic set as time goes on. These are the central results of the paper and open the possibility for interpreting fractal structures appearing in streaklines visualizations of flows, in general, as signs of Lagrangian chaos. Since the convergence to the unstable manifold is exponentially fast, we approached this manifold by simply following streakline segments for a few periods of the flow. The stable manifold was obtained in an analogous manner from the time reversed Lagrangian dynamics. We then construct the chaotic set and show, in a series of pictures, how the chaotic set and its manifolds change with time. In Section 6 we describe how characteristic numbers of the chaotic dynamics around the strange set can be extracted by following the motion of line segments. Section 7 is devoted to the time delay statistics that is dominated asymptotically by trajectories remaining for a long time near to the surface of the cylinder. On short time scales, however, the effect of unstable periodic orbits can also be seen in the appearance of an exponential decay. A quantity providing a more detailed description, the time delay function is discussed in Section 8. The most remarkable structures in it are also given by trajectories of particles directly colliding with the cylinder, but the fine structures reveal information about the chaotic set. Eigenvalues of short periodic orbits can be extracted from scaling properties of this function. The last section gives a summary of quantitites that could be measured in a laboratory experiment.

2. Chaotic scattering: a brief survey

In this section we summarize briefly the most important features of chaotic scattering. For more details we refer to the review papers [30–33].

Because of the asymptotic simplicity of the motion, scattering *trajectories* can have compli-

cated shapes mainly in a finite region of the configurational or phase space, in the so-called interaction region. Consequently, chaos is restricted to finite time scales and chaotic scattering is, in fact, a special appearance of transient chaos [32].

In chaotic scattering, just like in any other chaotic processes, there exists an *infinity of unstable periodic orbits*. Unstability means that they are either hyperbolic with a positive maximal local Lyapunov exponent or marginal with zero maximal Lyapunov exponent. In fact, the number of periodic orbits increases with their period *exponentially*, and the *topological entropy* K_0 tells us how rapid this increase is. Periodic orbits provide a backbone of the scattering process in the sense that the particle might remain close to a periodic orbit for a while, then leaves it and comes to the vicinity of another one, and so on. The motion can be considered as a random walk among periodic orbits.

It is also known from earlier studies that some short *basic periodic orbits* play a fundamental role. More complicated ones turn out to be *shadowed* by these basic ones which means that any periodic orbit can be built up from segments of the basic periodic orbits. Long lived scattering trajectories remain close to the periodic ones and, consequently, their segments inside the interaction region can also be shadowed by the basic periodic orbits [47–49]. In investigations of chaotic scattering the determination of the shortest and simplest periodic orbits is of outstanding importance.

In chaotic scattering processes there exists a *nonattractive chaotic set*, sometimes called chaotic saddle. It is an invariant set in phase space, and consists of all the unstable periodic orbits lying in the interaction region and their heteroclinic and homoclinic connections.

The chaotic set possesses a *stable manifold* along which trajectories can reach the set itself. The stable manifold of a given periodic orbit is practically indistinguishable from that of the complete set. The stable manifold has zero measure and provides a *fractal* foliation of the phase space. This is why a particle has zero probability to be trapped forever by a periodic orbit, or by the entire chaotic set.

Analogously, the chaotic set also has an *unstable manifold* which is the stable manifold in the time reversed dynamics. The unstable manifold is also an infinitely long line that foliates certain regions of the phase space in a fractal manner.

The chaotic set itself is the common part of its stable and unstable manifolds and exhibits thus a fractal structure along both the stable and the unstable direction. Because of the Hamiltonian character, the fractal dimension of the chaotic set has the same value, D, along both directions [32]. The chaotic motion on the invariant set is characterized by an average Lyapunov exponent $\bar{\lambda} > 0$ which can also be extracted from typical scattering trajectories of particles that never hit the set exactly but come close to it.

If stable (elliptic) periodic orbits are also present, they are surrounded by elliptic islands containing quasiperiodic orbits, and can thus never be accessed by scattering trajectories. What is accessible is the surface of the island, a KAM surface, that contains a lot of periodic orbits which can be arbitrarily weakly unstable. The presence of a KAM surface or any marginally stable orbit leads to the appearance of a so-called *nonhyperbolic* component of the chaotic set that is responsible for an anomalous long time behaviour. It is also known that the partial fractal dimension D of the chaotic set is then approaching 1 with an ever refining resolution [50].

Incoming trajectories escape sooner or later the interaction region. The statistical behaviour of the survivors is an important characteristics of chaotic scattering. One is interested in the *time delay statistics* that tells us how the probability for finding a trajectory in the interaction region decays with the time spent there. If the chaotic set is hyperbolic, i.e. does not contain any marginally stable component, this decay is exponential. The number characterizing the

decay is the *escape rate* κ, the reciprocal value of the avarage chaotic lifetime in the system. In nonhyperbolic situations the decay is much slower, of algebraic type. If both hyperbolic and nonhyperbolic components are present, a crossover may be observed from an initial exponential decay to an asymptotic power law behaviour [51].

Another central object in the theory of chaotic scattering [30–33] is the *time delay function* describing how the time spent in the interaction region depends on the initial conditions. This provides a more detailed description than the time delay statistics. The time delay function takes on an infinite value whenever the initial condition falls on the stable manifold of the chaotic set. The infinities in the time delay function thus appear in a fractal pattern that has the same dimension D as the partial dimension of the chaotic set. A study of the time delay function also provides the possibility to obtain any other important characteristics of the chaotic set [52,53].

3. Flow behind a cylinder in a channel

We investigate the Navier-Stokes flow in an infinite channel of width w with a circular cylinder of radius R placed into the middle of the channel. An incompressible viscid fluid moves through the channel with an average velocity u_{av} from the left to the right. The flow is characterized by two free parameters: by the Reynolds number $Re = 2Ru_{av}/\nu$, where ν is the viscosity, and by the aspect ratio $r = R/w$. We will consider sufficiently small Reynolds numbers Re only, for which the flow is essentially 2-dimensional. We assume that the velocity of the fluid is sufficiently small such that far away in front and far away behind the cylinder a parabolic velocity profile is created. For Re below a critical value, which lies slightly below 80 in our case, the flow becomes stationary in the long time limit. In the following we concentrate on the next range of Reynolds numbers where an exactly *time periodic flow* of some period T_c occurs (see [74,73])

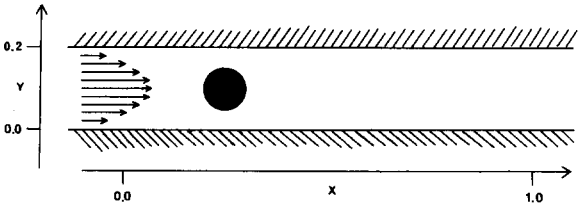

Fig. 1. Geometry of the channel and the cylinder within. The walls of the channel are at $y = 0$ and $y = w = 0.2$. The center of a cylinder of radius $R = 0.05$ is placed at $(0.25, 0.1)$. The arrows inside the channel indicate the incoming parabolic velocity profile.

Behind the cylinder vortices are created. Later they detach from the cylinder and drift along the channel. After some distance they are suppressed by viscosity. We obtain a typical vortex sequence of finite length. In a narrow channel (r is not very small compared to one) the vortex sequence is strongly damped and quite short. In our case we have *at most two* different vortices at one instant of time.

Fig. 1 shows the geometry we use and the incoming parabolic velocity profile. It is valid rather close to the cylinder and so it was sufficient for the following to choose this profile as initial condition along the line $x = 0.0$. The results shown below are obtained for $Re = 250$ and $r = 0.25$ which lead to $T_c = 1.107$. Similar numerical results for $Re = 80$ are given in [24,29].

Fig. 2 gives a plot of the instantaneous streamlines of the Navier-Stokes flow at time $t = 0$ mod T_c and at time $t = T_c/4$ mod T_c where the zero of time has been chosen arbitrarily. Because of the symmetry of the geometry we use, and because of the solution, the streamlines for $t_2 = t_1 + T_c/2$ can be obtained by reflecting the streamlines plot belonging to time t_1 about the symmetry axis of Fig. 1. Thus, for example, the streamlines for $t = T_c/2, 3T_c/4$ can easily be generated from those shown in Fig. 2.

We can thus imagine the time development of the velocity field. Behind the cylinder two vortices are created within any time interval of length T_c, one in the upper half and the other

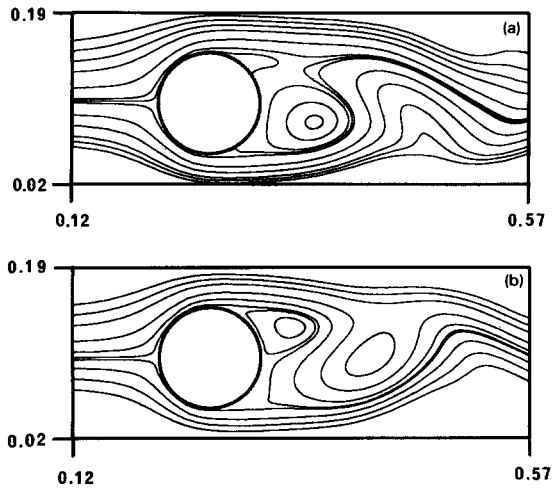

Fig. 2. Streamlines obtained from a numerical solution of the Navier-Stokes equations for $Re = 250, r = 0.25$ at time t mod T_c, where (a) $t = 0$ and (b) $t = T_c/4$.

one in the lower half of the channel. These two vortices are delayed by a time $T_c/2$. The vortices first grow in size, then they separate from the cylinder and start to drift along the channel. Now the viscosity of the fluid and the presence of the walls of the channel become important for their destabilisation and destruction after a short length of travel.

The principal approach to the determination of the velocity field or of the stream function is a solution of the Navier-Stokes equations. We used a method based on the one described in [54] and modified according to [55] (see [72]). A grid of size 42×202 in position space has been taken and the average temporal resolution provided by the numerical procedure was $0.003\, T_c$. The relaxation to the asymptotic periodic behaviour required a CPU time of several hours on a CDC vector computer, Cyber 205. As input for the Lagrange dynamics this velocity field was stored over half a time period on an equidistant space-time grid where the time step $0.03\, T_c$ has been chosen. Several tests have been carried out to check (both in space and time) the grid-independence of the Navier-Stokes solution and the reliability of the simulated particle dynamics.

Because of the restrictions in the computer resources and resolution, this method is not suitable to investigate very fine details of the dynamics. For this purpuse, we constructed an analytical model, fit, of the stream function [27] which contains useful qualitative features of the Navier-Stokes flow and provides the opportunity to have very good resolution. This model is presented in the Appendix.

Where available, we shall give below the results obtained from the Navier-Stokes flow, but in certain cases, when the required high precision was not reachable by the direct simulation, the results of the model will be shown (for details we refer to [27]). In the figure captions we indicate how the results displayed were obtained.

4. Trajectories and periodic orbits

The motion of particles inside the vortex sequence can qualitatively be understood as follows: In time-independent velocity fields, the particle trajectories coincide with the streamlines. Then it would be impossible for a particle ever to enter a vortex from outside or to leave it from inside. However, when the velocity field is time-dependent, the position of the vortices changes relative to the particle and the particle can be overrun by a vortex and come inside of it. After a while the particle may be left behind the vortex again. If it leaves the vortex just at the appropriate time and at the right place, then it may be overrun by the next vortex and be trapped by it for a while, etc. So a particle can be handed over from one vortex to the next one and stay in the region behind the cylinder for a long time, even though each individual vortex leaves this region quite soon. For this effect to occur, it is necessary that the particle motion is synchronized to the vortex motion such that inside the growing and moving vortex the particle is moved from the front, where it is captured, to the back of the vortex, where it is released again.

We followed the particle trajectories in contin-

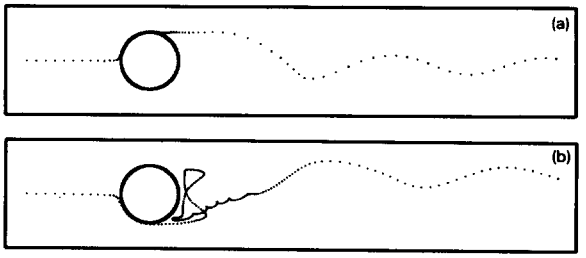

Fig. 3. Two particle trajectories in position space based on Navier-Stokes data. (a) shows a scattering trajectory moving along the wall of the cylinder in very close distance. (b) shows a trajectory which comes close to periodic orbits and is overshadowed by them in the vortex containing region.

uous time to have the freedom to take a snapshot at any time. If one is interested just in a stroboscopic map at one specific time mod T_c, then the simple method proposed in [56] could be used succesfully to locate e.g. the periodic points in the stroboscopic plane.

Particle trajectories can be of different type. Some of them directly approach the wall of the cylinder where the velocity field goes to zero. Then the particle passes along the cylinder surface very slowly until it separates again on the back side. Such a trajectory is shown in Fig. 3a. With other initial conditions, the particle can be trapped by the vortices for a while and performs a complicated, chaotic looking motion (Fig. 3b). (For some particle trajectories in the wake of a rectangular cylinder see [18].) We note that complicated particle trajectories occur in spite of the fact that the streamlines are *smooth* (cf., Fig. 2). This is in analogy to complicated trajectories appearing in the phase space of Hamiltonians of simple functional form.

In order to understand the complicated behaviour of long scattering trajectories, it is necessary to study the properties of periodic and localized orbits in the system. The simplest truly periodic orbits are plotted in Fig. 4. Two asymmetric period-one orbits are plotted by dotted lines. For better distinction, a third period-one orbit which is of figure eight shape is plotted as a solid line. It is clear that the trajectory of Fig. 3b is shadowed for a while by the asymmetric

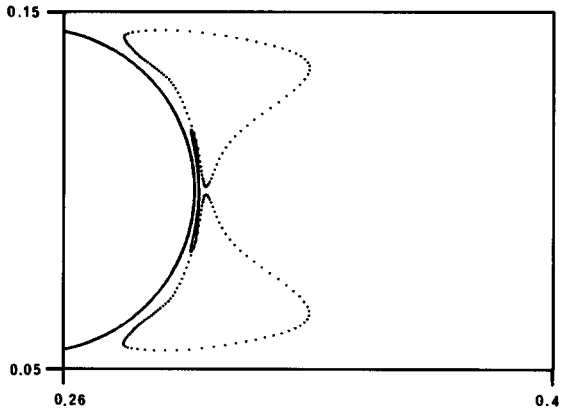

Fig. 4. Plot of the period one orbits (Navier-Stokes data). The two large orbits are drawn by dotted lines, where two consecutive points are separated by a time of $T_c/100$. The third small figure eight orbit is drawn by a solid line for better distinction.

period-one orbits. It has to be emphasized that the period-one orbits are rather unstable. Their eigenvalues are on the order of 1000, much larger than in the paradigm examples of point mechanical chaos.

Another basic feature, which can best be seen with the enhanced resolution of the model flow (given in the Appendix), is that a sequence of period 2,3, and 4 orbits, which have been found (Fig. 5a,b,c), are shifted with increasing period closer and closer to the wall. Their forms suggest that they are partially shadowed by a period-one orbit and partially also by segments lying close to the wall. Computing their eigenvalues λ_n, where n is the period, we found that $\ln(\lambda_n)/n$ decreases with n. By taking into account that the cylinder surface is the union of degenerate parabolic points with Lyapunov exponent zero, we can conclude that the wall plays the role of a *basic periodic orbit of marginal stability*. In this respect it is similar to a KAM surface. The boundary of the latter is, however, a complicated fractal structure in contrast to the surface of the cylinder.

We thus conclude that short periodic orbits are *not* sufficient for carrying out the shadowing process. In addition, the wall of the obstacle consisting of a continuum of parabolic points has

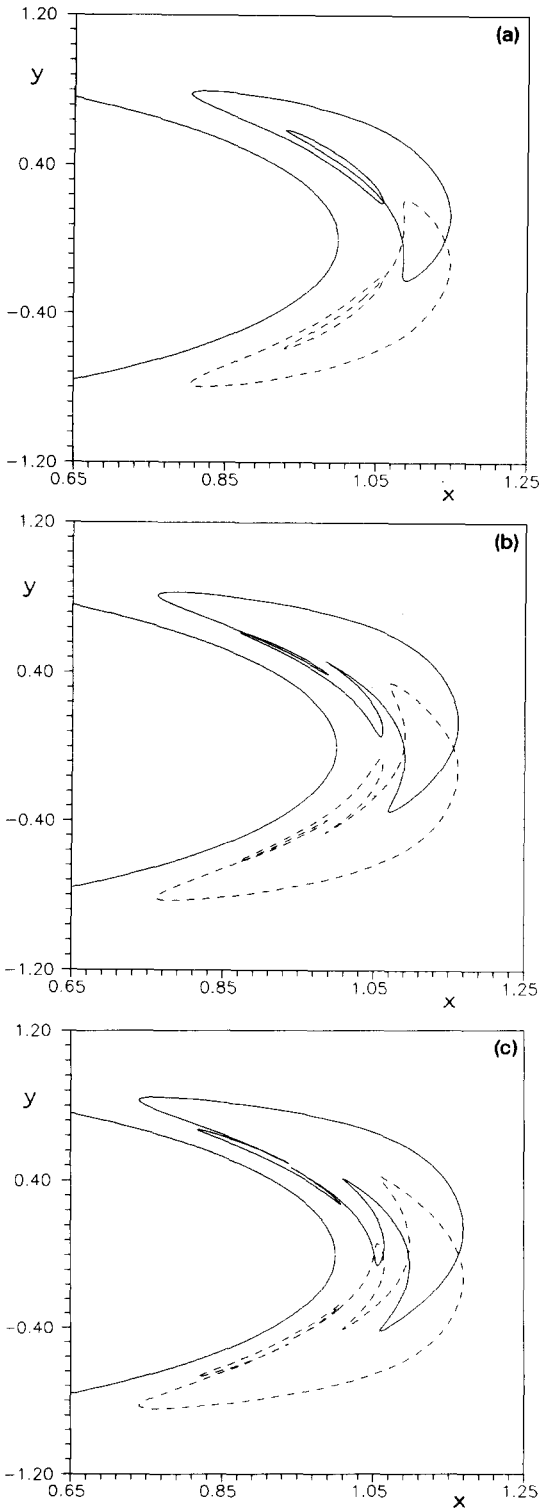

Fig. 5. Simple periodic orbits of higher order. (a),(b), and (c) show periodic orbits of period 2, 3, and 4, respectively. These plots are based on the flow of the analytical model (for more details see [27]). For better visualization, different scales has been used on the axes.

to be included as it acts like a *further basic periodic orbit*. In fact, very long periodic orbits can come arbitrarily close to the wall. So we can define two components of the invariant set: a *hyperbolic* component containing the short hyperbolic orbits as well as the ones shadowed by them alone, and a *nonhyperbolic* component, containing the wall as well as periodic orbits shadowed partially by the wall. In our numerical computations we did not find KAM surfaces, but on general ground their existence is expected eventually on extremely small scales. KAM surfaces also belong to the nonhyperbolic component.

5. Streaklines, invariant manifolds and the chaotic saddle

Let us imagine that we inject particles into the flow in front of the cylinder. If the point of injection (x_{in}, y_{in}) is not close to the stable manifold of the front stagnation point or of the chaotic set, then the injected particles will not be trapped and will be advected away by the flow quite rapidly. If the point of injection is close to the stable manifold of the front stagnation point, particles will be sticked to the surface of the cylinder for a long time. If, however, the point of injection happens to lie close to the stable manifold of the chaotic set, the particle will be attracted, because of the stable foliation, to a vicinity of the set where it spends a finite amount of time, and escapes finally *along the unstable manifold* of the chaotic set. Therefore, we conclude that dye particles remaining for a few periods behind the cylinder will draw out the unstable manifold of the chaotic set.

Consequently, the fractal structures seen in flows behind obstacles by means of dye visualization can, in general, be interpreted as *unstable manifolds of chaotic sets*. This is in analogy to the results of Ottino and coworkers [4] obtained in closed flows showing that dye particles move asymptotically along unstable manifolds of periodic orbits embedded in the chaotic see.

Streaklines, often used in flow visualization [35,16,57], are the set of points reached, at a given instant of time, by a continuum of particles injected at a given point into the flow at any previous time before. Consequently, our general observation is that those *segments of the streaklines* which remain in the wake of an obstacle for a long time and exhibit fractal character *coincide with the unstable manifold of a chaotic set* existing behind the obstacle. This is a slight conceptual extension of the result of Shariff, Pulliam and Ottino [22] who emphasized the importance of the stagnation points' unstable manifold. We claim that it is the *complete* chaotic set whose unstable manifold is relevant for the streaklines. In fact, the unstable manifold of the stagnation point(s) is expected to come arbitrarily close to that of any periodic orbits. These manifolds together (more precisely, their closure) form the unstable manifold of the chaotic set. Many streakline patterns found in different fluid mechanical problems before [35,57,16] provide thus evidence for the chaoticity of the passive advection in that system.

We describe here a numerical method for computing streaklines that also enable us to extract quantitative characteristics of the chaotic set, like, e.g., topological entropy and Lyapunov exponents. As pointed out above, the chaotic set contains both hyperbolic and nonhyperbolic components. We expect that the crudest fractal structures of streaklines reflect the presence of the strongly unstable periodic orbits and the hyperbolic part. By intersecting the streaklines with smooth curves one should thus obtain a fractal dimension strickly less than unity. When increasing the resolution, one should see, however, the nonhyperbolic part and a crossover of the fractal dimension to unity. In the numerical plots shown below we just see the large-scale structures corresponding to the hyperbolic influence.

The convergence along the stable foliation toward the unstable manifold is given on short time scales by the rule $\exp(\bar{\lambda}_2 t)$ where $\bar{\lambda}_2$ is the negative average Lyapunov exponent of the hyperbolic component of the chaotic set. Because of the Hamiltonian structure, however, $\bar{\lambda}_2$ is just the negative of the positive average Lyapunov exponent $\bar{\lambda}$.

In order to determine the streaklines numerically, we select a suitable point in position space and insert particles at this point into the flow with a constant rate which is on the order of 1000 during a period T_c of the velocity field. The trajectories of all these particles are followed. At any instant of time, if the distance between two adjecent particles increases above a threshold value of 5×10^{-4} a new particle is inserted at the midpoint between the two already existing ones. This is done in order to obtain numerically a continuous appearance of the streaklines. Thus, the number of particles is proportional, on the average, to the length of the streakline. The chaotic properties of the dynamics are reflected in the appearance of an exponential growth of the length of the lines and, consequently, also of the number of the interpolated particles. This will allow us to extract qualitative characteristics of the saddle as will be discussed in the next section. The addition of interpolating particles in an experiment is neither possible nor necessary because of the macroscopically large number of dye particles.

Since the streaklines converge to the unstable manifold of the chaotic saddle, we approached the latter numerically by simply following a segment of the streakline up to a sufficiently long time. In our case a duration of about $3T_c$ was sufficient. The stable manifold is obtained by exactly the same method using the time-reversed Lagrange dynamics. This is of course not possible in an experiment, but the stable manifold can also be obtained by distributing an ensemble of particles around the cylinder and plotting the initial position of only those particles that remain in this region for a long time [58,51]. One might also speculate about interpreting the stable manifold as a kind of fractal basin boundary [59] that would enable us to take over methods

Fig. 6. (Above) Streaklines of the Navier-Stokes flow. (a) gives the complete streakline at time $t = 3T_c + 0.1$ of particles injected at $(x_{in}, y_{in}) = (0.25, 0.155)$ since $t = 0$. The orange segment corresponds to particles injected in the time interval between $3T_c$ and $3T_c + 0.1$. The green and blue segments correspond to injections in the interval $(2T_c, 3T_c)$ and $(T_c, 2T_c)$, respectively. (b) shows only that part of the streakline which has been injected in the time interval $t \in [0, T_c]$. The close proximity between the blue segment in (a) and the total structure of (b) reflects a rapid convergence. The overlap of the green and blue segments resulting in a dark color in (a) is also a sign of rapid convergence. Taking longer times between injection and observation would not modify the structure shown in (b) which coincides practically with the unstable manifold W^u of the chaotic set. The frames show the region $(0.26 < x < 0.6, 0.035 < y < 0.165)$.

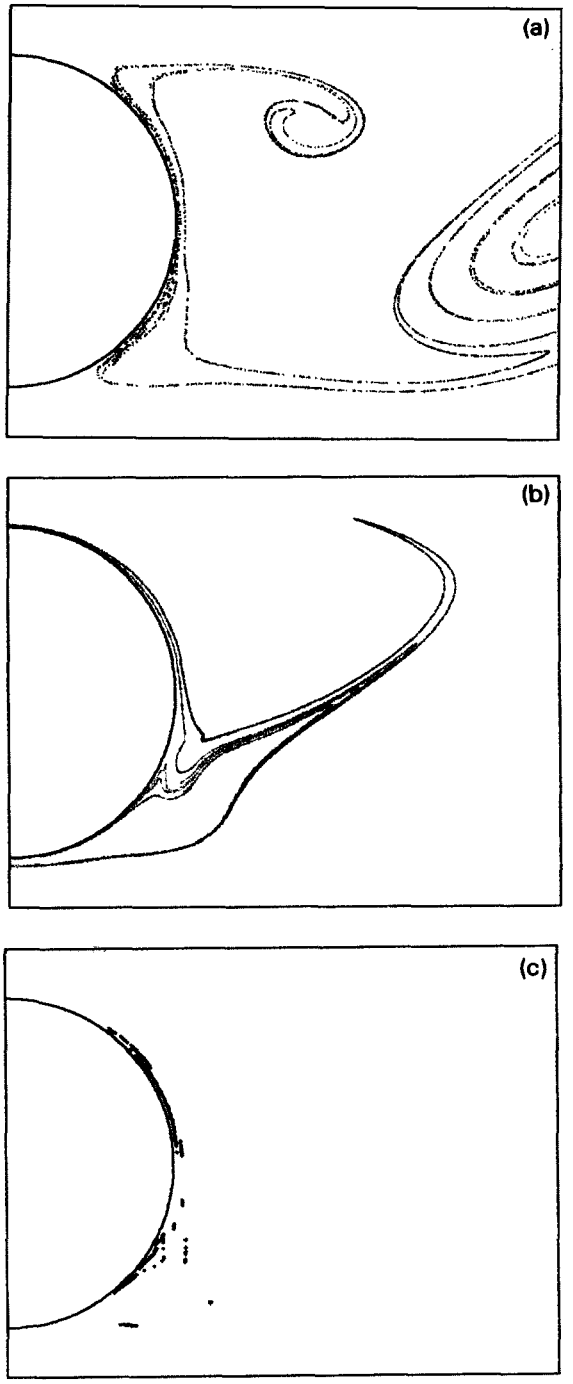

Fig. 7. (Right) The chaotic set and its invariant manifolds. (a) gives a similar segment of the streakline as Fig. 6b but taken at time $2T_c + 0.6$ injected in the time interval $(0, T_c)$. (b) gives the streakline of the time reversed Lagrangian dynamics. The part of the line which has been injected at $(x_{in}, y_{in}) = (0.35, 0.1)$ in the time interval $t \in [0, T_c]$ has evolved until time $t = 3T_c - 0.6$ (the sum of forward and backward times must be an integer multiple of T_c in order to obtain matching pictures). It is a good representation of the stable manifold W^s of the chaotic set. (c) gives the intersection of the manifolds W^u and W^s representing the chaotic set Λ at time $t = 0.6 \bmod T_c$. The region shown is $(0.25 < x < 0.42, 0.035 < y < 0.165)$.

from this branch of nonlinear dynamics.

The choice of the injection point is conveniently chosen, in case of streaklines or unstable manifolds, if it lies close to the stable manifold. Naturally, when constructing the stable manifold by means of the time-reversed Lagrange dynamics, the injection should take place in the vicinity of the unstable manifold.

In Fig. 6 we demonstrate pictorially how parts of the streaklines converge towards the unstable manifold W^u of the chaotic set. Starting from the time $t = 0$ particles are injected at the point $(x_{in}, y_{in}) = (0.25, 0.155)$. Fig. 6a shows the streakline thereby created at time $t = 3T_c + 0.1$. That segments of the streakline which have been injected in the time intervals $(T_c, 2T_c)$, $(2T_c, 3T_c)$ and $(3T_c, 3T_c + 0.1)$ are shown in blue, green and orange, respectively. The segment injected in the time interval $(0, T_c)$ is shown separately in Fig. 6b in red. We see that the red segment gives essentially the same structure as the blue segment only filled in a little bit more densely. In this sense we can consider the red segment to represent within our numerical resolution already the limiting structure towards which the streaklines converge in the long run. This limiting structure is just the unstable manifold W^u. In [29] we give for another value of the Reynolds number a comparison between the streaklines and a direct construction of several thousand points of W^u and found good coincidence of the structure.

By running the Lagrangian dynamics backward in time (with the same velocity field of course) we can obtain in the same way a faithful representation of the stable manifold W^s of the chaotic set, when we inject the particles at a point behind the cylinder. For the numerical computations we have chosen $(x_{in}, y_{in}) = (0.35, 0.1)$ for the reversed dynamics.

In the knowledge of the invariant manifold one can easily obtain the chaotic set Λ as their intersection. Alternatively, even if the manifolds are not known, the chaotic set could be constructed by using an ensemble of particles. This is obtained by monitoring, after discarding the transients, those trajectories only that remain for a long time, as described in [61,58,51].

Fig. 7 shows a comparison of W^u, W^s and Λ at the time $t = 3T_c + 0.6$. Part (a) of the figure displays again a similar structure as Fig. 6b, only in a smaller frame in order to magnify the most interesting parts. Fig. 7b exhibits the corresponding stable manifold. In Fig. 7c the intersection points between W^u and W^s are marked to represent the invariant set Λ itself.

Because the Lagrangian dynamics is explicitly time-dependent, also the positions of W^u, W^s and Λ are explicitly time-dependent and are periodic with the period T_c of the velocity field. Fig. 8 gives the positions of W^u and W^s for times $t = 0.6 + k \times 0.1 \bmod T_c$ where $k = 0, ..., 5$ in parts (a), ..., (f), respectively. W^u and W^s are shown in red and blue, respectively. It is sufficient to show the time evolution of these sets over half of a period, because at time $t_2 = t_1 + T_c/2$ all these sets are just the mirror images of the corresponing sets taken at time t_1 where the line of reflection is the symmetry axis along the channel. In Fig. 9 we display in a smaller frame the invariant set Λ, i.e. the intersection between W^u and W^s where the positions of the periodic orbits shown in Fig. 4 are also marked. Again parts (a), ..., (f) belong to times $t = 0.6 + k \times 0.1 \bmod T_c$ for $k = 0, ..., 5$, respectively. As Fig. 9 suggests, the points of the chaotic set *accumulate* on the surface of the cylinder. Since the chaotic set has to be closed, we conjecture that the entire *cylinder surface* between the two unstable stagnation points, including these stagnation points themselves, belongs to the chaotic set.

6. Characteristic numbers

As mentioned in the previous section, the numeric procedure used to plot the streaklines has been carried out by adding interpolating particles. This is not only a useful way for keeping the density of particles constant along streaklines, but the rate at which particles have to be added expresses an essential property of chaos: exponential stretching and folding. The growth rate of the particle number can thus be connected with basic chaotic characteristics.

To see this, take any finite two-dimensional region A behind the cylinder that contains parts of the invariant set. The total number of particles

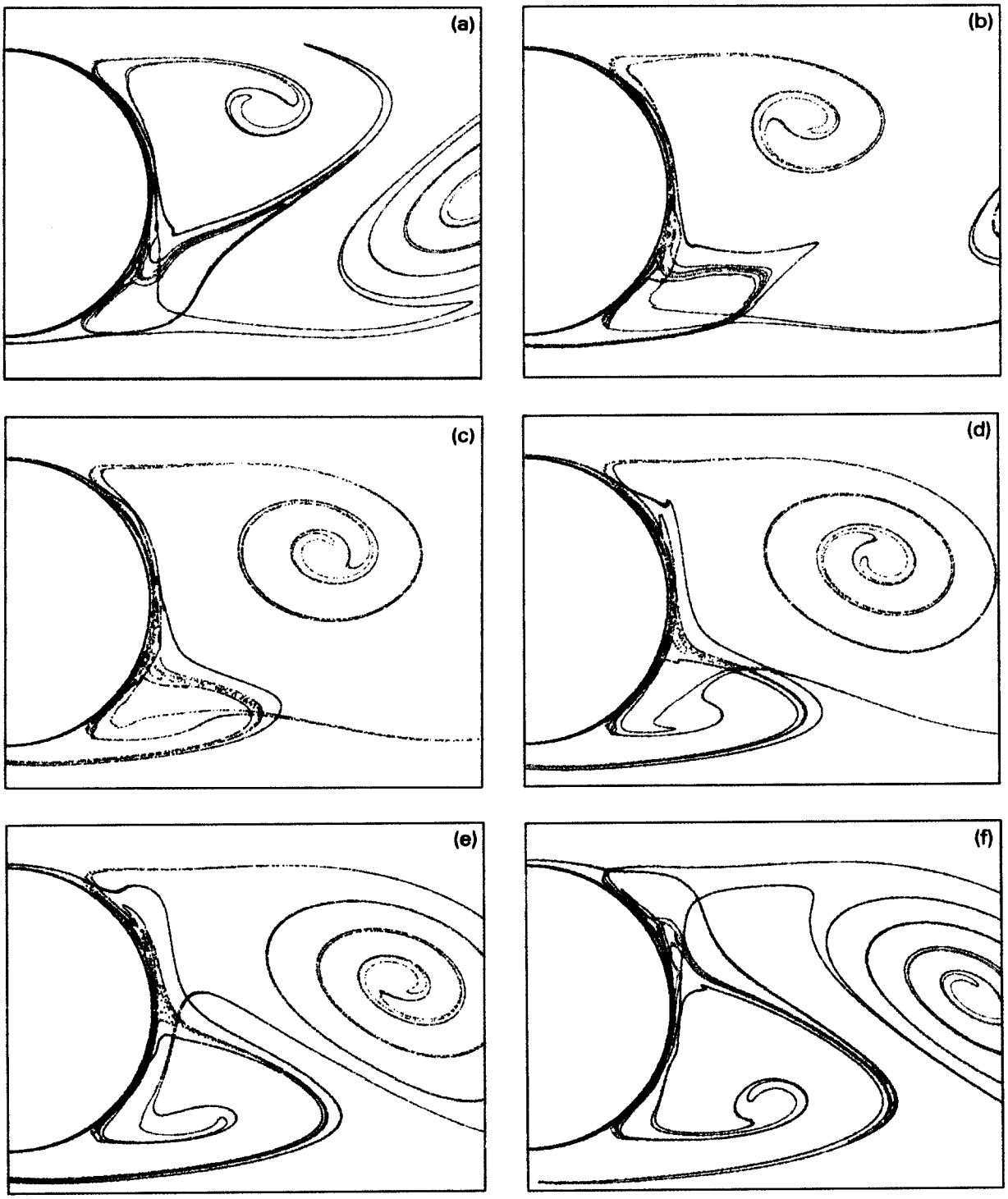

Fig. 8. Time development of invariant manifolds (Navier-Stokes data): W^u (red) and W^s (blue). Parts (a)–(f) correspond to times $t = 0.6 + k \times 0.1 \bmod T_c$ where $k = 0, \ldots, 5$. It is easy to imagine the continuation of this series by using the symmetry property mentioned in the text.

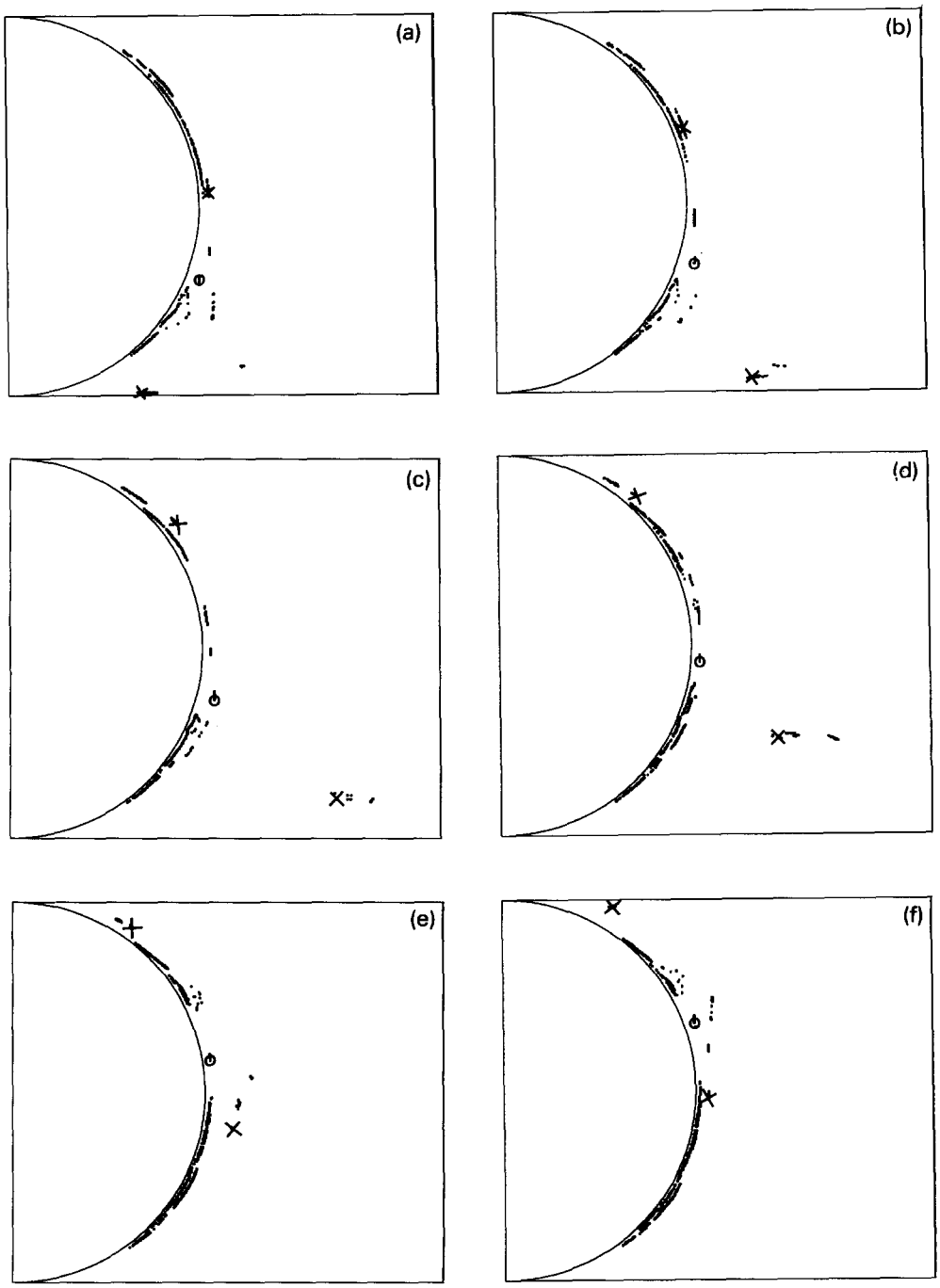

Fig. 9. Time development of the chaotic set A. (a)–(f) correspond again to times $t = 0.6 + k \times 0.1 \bmod T_c$ $(k = 0, ..., 5)$. A is obtained as the intersection between W^u and W^s (see also the black dots in Fig. 8.) The frames correspond to the region $(0.25 < x < 0.36,\ 0.05 < y < 0.15)$. Here circles mark the position of the figure eight orbit (shown in Fig. 4 with continuous line). The location of the upper and lower period-one orbits (dotted lines in Fig. 4) are denoted by crosses.

inside, as well as the total length and the number of connected components, all grow with the same exponent. It is well-known that the folding property of chaos is quantified by the *topological entropy* being the growth rate of how rapidly the number of foldings increases when time goes on (cf., e.g, how rapidly the number of branches in an n-fold iterated map increases with n), see also [60]. Therefore, we conclude that the common growth rate of all the exponentially increasing quantities related with region A is the topological entropy of the saddle. In particular, let $M(t)$ denote the number of particles used in the creation of the streakline inside the selected region at time t. The topological entropy K_0 of the chaotic saddle can then be extracted from $M(t)$ via the relation

$$M(t) \sim \exp(K_0 t/T_c), \tag{3}$$

which holds for sufficiently large time. We found nice scaling for $t > 2T_c$. Note that K_0 as defined above is the topological entropy of the stroboscopic map since time is measured in units of T_c.

The value of K_0 obtained by this method is completely independent of the choice of the region A since the rate of folding is the same in the vicinity of any point. We choose for A the section of the channel lying between $x = 0.25$ and $x = 1.0$. In Fig. 10 the logarithm of the total number of particles inside A is plotted versus time obtained from Navier-Stokes data. This plot has some periodic oscillations with a period of $T_c/2$ around a straight line of slope 1.7. So we obtain the value $K_0 = 1.7$ from the dynamics of the streaklines.

Another quantity characterising stretching rather than folding can be obtained by following two neighbouring particles in a streakline over a short time Δt. Let l_i denote the distance between two neighbouring particles on the streakline at time t. The growth rate of the distance during Δt is $1 + \Delta l_i/l_i$ where Δl_i is the increase of the distance between the neighbouring particles. Thus, we can consider the quantity $\Delta l_i/(l_i \Delta t)$ to be a local stretching rate λ_i. The probability to find

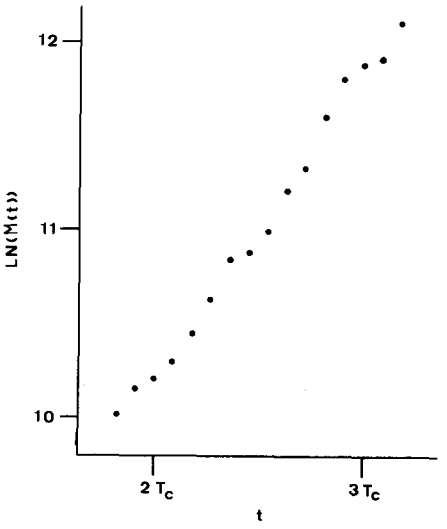

Fig. 10. Logarithm of the number of particles in the streakline versus time in the region $0.25 < x < 1$ of the Navier-Stokes flow. The average slope gives the value 1.7 for the topological entropy K_0.

this exponent in a randomly chosen point along a streakline of total length L inside the selected region is l_i/L. Taking the average of the λ_i's with this probability, an average stretching rate $\bar{\lambda}$ is obtained as

$$\bar{\lambda} = \frac{T_c}{L}\frac{\Delta L}{\Delta t}, \tag{4}$$

where $\Delta L \equiv \sum_i l_i$ is the full increase of the streakline's length inside the region. The factor T_c reflects again that time is measured in units of the period of the velocity field. In the limit $\Delta t \to 0$ the right hand side is proportional to the logarithmic derivative of L.

Note that the average stretching rate as defined above might depend on the region selected. If the region A is a good cover of the invariant set, in particular of the strongly hyperbolic periodic orbits, and if it does not contain too large parts far away from the invariant set, then $\bar{\lambda}$ can be interpreted as the *Lyapunov exponent of the hyperbolic component*. This is also consistent with the fact that the probability with respect to which the average is taken above corresponds to the natural measure of hyperbolic chaotic sets

[32].

By choosing A to be the region between $x = 0.25$ and $x = 0.5$ we obtained in the Navier-Stokes flow $\bar{\lambda} = 4.7$. Note that this number is definitely less than the Lyapunov exponents of the period one orbits (shown in Fig. 4) which are on the order of approximately $\ln(1000) = 6.9$. This shows that longer periodic orbits can be less unstable than the period one orbits even if they belong to the hyperbolic component. The relatively large value of $\bar{\lambda}$ ensures that the convergence of the streaklines to the unstable manifold is perfect within a time of $2T_c$ (cf. Fig. 6).

From the dynamics of the streaklines the escape rate κ can also be extracted as follows. At time $t = T_s$ we stop to inject new particles at the point (x_{in}, y_{in}) and at the same time we stop to interpolate particles into the moving and stretching particle chain. Then most streakline segments disappear quite rapidly out of the area A under observation. The few remaining segments are stretched and become filled with particles very sparsely only. The number M' of remaining particles inside A decreases like

$$M'(t) = M'(T_s)\exp[-\kappa(t - T_s)/T_c] \qquad (5)$$

on the average. By this method we have found the value $\kappa = 3.2$.

Having obtained an estimate for the escape rate and the Lyapunov exponent, we can use a famous relation [61] expressing the partial information dimension D_1 along the invariant manifolds of the chaotic set as

$$D_1 = 1 - \kappa/\bar{\lambda}. \qquad (6)$$

With values determined above we obtain $D_1 = 0.32$ which can be considered as a good estimate for the partial fractal dimension D of the chaotic set, or equivalently for the fractal dimension of the intersection accross the unstable or stable manifold. This number shows that the intersection is a rather sparse fractal which agrees with what one sees on the pictures. Furthermore, the metric entropy K_1 is the product of the information dimension D_1 and the Lyapunov exponent [61]. Thus we find $K_1 = 1.5$ which is a value somewhat below that of the topological entropy $K_0 = 1.7$ as it should be.

7. Time delay statistics

For a scattering system it is essential to give a proper labelling of asymptotes. In our system this can be done as follows: Pick a particular value x_{in} of x in the incoming asymptotic region (in the Navier-Stokes case we shall take $x_{in} = 0.02$) and record the y-coordinate and the time modulo T_c at which the particle coming from $-\infty$ crosses the line $x = x_{in}$. These two numbers y_{in} and t_{in} label any incoming asymptote uniquely.

Because the trajectories we follow start and end close to the middle of the channel, they would need a time T_0 to run from x_{in} to x_{out} in the absence of the cylinder. Since in a parabolic profile the velocity in the middle of the channel is $u_0 = 1.5u_{av}$, where u_{av} is the average velocity, we find $T_0 = (x_{out} - x_{in})/u_0$. So we define the time delay of a particle trajectory as $\delta t = DT - T_0$ where DT is the actual time the particle needed to proceed from x_{in} to x_{out}. Then the value of δt is independent of the choice of x_{in} and x_{out} as long as these two values of x are located in the asymptotic region. We measure the number of particles $N(\delta t)$ starting in x_{in}, y_{in} and having a time delay larger than δt, where the initial time t_{in} is distributed evenly.

Fig. 11 gives a plot of $\ln(N(\delta t))$ versus $\ln(\delta t)$ obtained from a large ensemble of trajectories. For large δt we see an algebraic decay, $N(\delta t) \sim (\delta t)^{-2}$. This behaviour is caused by the wall of the cylinder and can be understood as follows: Both in the Navier-Stokes computation and in the analytical model we impose no slip conditions on the surface of the obstacle since we are dealing with viscous fluids.

This condition implies that the tangential component of the velocity goes to zero linearly when approaching the wall. Accordingly, the value of ψ goes to its value ψ_w on the wall

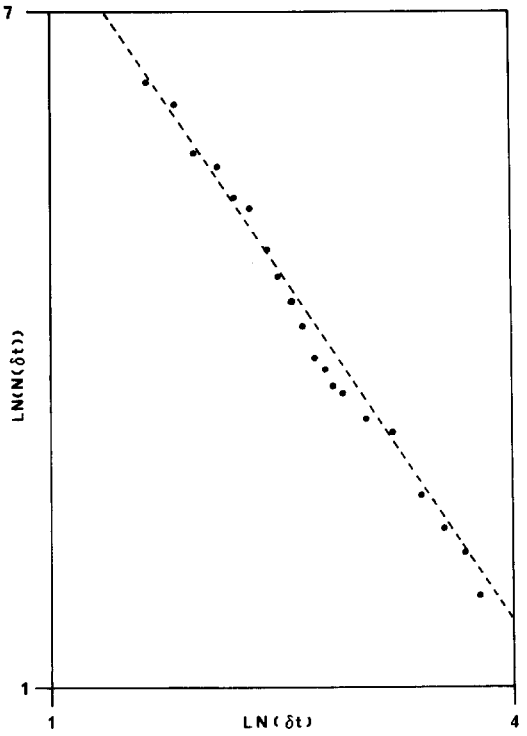

Fig. 11. Logarithm of the relative probability to find a trajectory with time delay larger than δt plotted versus ln (δt) in the Navier-Stokes flow. The slope of the straight line is -2. $y_{in} = 0.0995$ is kept fixed and the values of t_{in} are distributed evenly. The dominant algebraic deacy is due a direct collision of particles with the front stagnation point.

quadratically. Considering for a while a stationary flow, we can write

$$\psi(r = R + d, \phi) \overset{d \to 0}{=} \psi_w + A(\phi) d^2 \qquad (7)$$

where polar coordinates have been used with the origin in the middle of the cylinder. (Cf. Eq. (10) of the Appendix where $\psi_w = 0$.) Note, that this condition is in contrast to the well-known potential solution $\psi = (r - R^2/r)\sin(\phi)$ valid for the flow of an inviscid fluid around a cylinder which violates the no slip condition. (The quadratic behaviour of ψ near the wall has also been incorporated in the model flow of [62] which differs in some other aspects from our model (fit) even though it starts with a similar power series expansion in the direct neighbourhood of the wall.) Far away in the asymptotic region we have

$$\psi(x, y) = \psi_w + u_0 y \qquad (8)$$

where u_0 is the background flow in the middle of the channel. This asymptotics is exact for the analytical model and is approximate for the flow in the narrow channel as long as the point (x, y) is close to the middle of the channel. In the incoming asymptotic region y is the impact parameter b of the particle with respect to the cylinder. We can also view b as the distance of the incoming asymptote from the stable manifold of the front stagnation point. Applying Eqs. (7) and (8) to the same streamline, we see immediately that d is proportional to $|b|^{1/2}$. The time a particle needs to pass along the wall is proportional to $1/d$ where d is the minimal distance from the wall. If the impact parameter axis is covered evenly with incoming particles, then the relative probability to get an absolute value of the impact parameter smaller than $|b|$ is proportional to $|b|$. Accordingly, the relative probability to get a closest approach to the wall smaller than d is proportional to d^2 and the relative probability to get a delay time larger than δt is proportional to $(\delta t)^{-2}$. Now, in our case we do not have a time-independent system and we do not cover the impact parameter axis (y_{in}-axis) by particles. In the time-dependent system the stable manifold of the front stagnation point moves periodically in time and, therefore, an even covering of the initial time with incoming particles has the same effect as the even covering of the impact parameter in time independent systems. The behaviour $(\delta t)^{-2}$ is also expected in time-dependent flows where particles enter evenly distributed in time, as long as y_{in} is sufficiently close to the middle of the channel such that y_{in} is hit by the stable manifold of the front stagnation point at some values of t_{in}.

We note by passing that if the leading term in ψ were proportional to some power β of d, then by the same considerations we would obtain in the time delay statistics an algebraic behaviour $(\delta t)^{-\gamma}$ where $\gamma = \beta/(\beta - 1)$. In this

way a measurement of the time delay statistics could provide experimental information about the behaviour of the velocity field in the boundary layer around the obstacle.

Comparing the effect of a smooth torus with that of a KAM surface, we see that they both induce a nonexponential decay in the time delay statistics described by a power law $(\delta t)^{-\sigma}$. In the case of KAM tori the decay is slower because of their stickiness and one has found $\sigma \approx 1.5$ [63–69] which differs from the exponent $\sigma = 2$ characterizing the smooth surface of the cylinder.

As long as the Reynolds number is close to its bifurcation point at which a stationary flow pattern is replaced by a time-periodic one, the front stagnation point exhibits small amplitude oscillations, and consequently, its stable manifold is confined to a very narrow strip along the symmetry line of the channel. For initial conditions outside of this strip the time delay function is dominated by hyperbolic influences, a situation investigated in Ref. [24]. Note, however, that even in such cases there are some nonhyperbolic effects present. Because of recirculation, the particle can approach the attractive stagnation point in the back of the obstacle. Their effects could only be seen on very fine scales. Further away in the Reynolds number from the bifurcation point, nonhyperbolic effects become essential.

Even in the latter case, one has an opportunity for studying hyperbolic effects if initial conditions are taken so as to avoid a direct collision with the front stagnation point. Fig. 12 shows a typical example for such a situation based on the results obtained from the model flow. We see exponential decay for small values of the time delay. The arrow indicates a crossover value δt_c to an algebraic decay valid for large delay times. Thus, we conclude that nonhyperbolic effects can be observed on short time scales and reflect the presence of an infinity of strictly unstable periodic orbits. Methods worked out for characterizing hyperbolic point mechanical scattering processes can well be applied in this range [27]. The long time behaviour is, however, always dominated by the nonhyperbolic effect of the cylinder surface. The crossover value δt_c can strongly depend on the choice of initial conditions in position space.

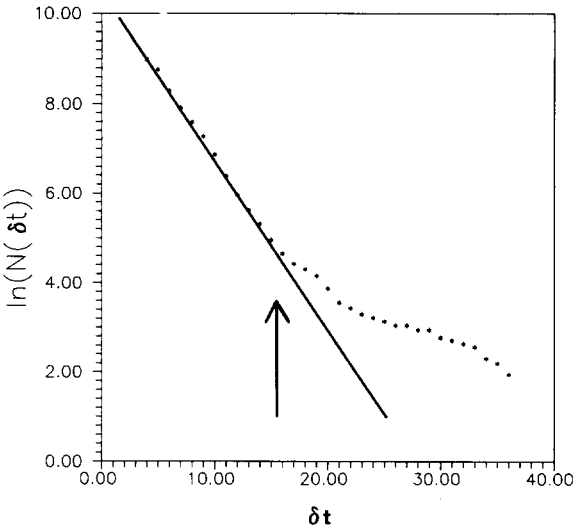

Fig. 12. Time delay statistics in the model system obtained by injecting particles at a point which avoids a direct collision with the front stagnation point. On short time scales an exponential decay can be seen with the escape rate κ of the hyperbolic component.

8. Time delay function

A clear criterion for scattering chaos is the occurence of a fractal set of singularities in the time delay function [70]. In our system this means in detail: Take a 1-dimensional subset of initial asymptotes, e.g. fix y_{in}, scan t_{in}, and plot the time δt of the particles.

Fig. 13a displays a representative example of δt as function of t_{in}. We see smooth parts and places where the function shows rapid changes, which are not well resolved on this scale. Fig. 13b gives a magnification with improved resolution of a part of Fig. 13a, and Fig. 13c gives a further magnification of an even smaller part. We observe a typical fractal construction: On any level of the hierarchy there are intervals of continuity and unresolved complements in between. On the next level we find new intervals of continu-

ity inside the so far unresolved parts. After every step of this construction there remain even smaller unresolved parts within those of the previous step. The set of accumulation points of the boundaries of intervals of continuity is a Cantor set. From level to level in this hierarchy the value of δt increases and on the fractal set itself the value of δt is infinite.

The big structures in the time delay function, the complete stems of Fig. 13, are caused by trajectories of the particles approaching the wall of the cylinder around the front stagnation point. Then they pass along the wall, just like in the example of Fig. 3a. As a consequence of the argument given for deriving the algebraic decay in the time delay statistics, the thick stems in the time delay function shown in Fig. 13 exhibit a one over square root singularity.

In this sense the coarse structure of the time delay is dominated by the effects of the wall of the cylinder. The effects of the unstable periodic orbits are to be found on finer scales, especially in the internal structure of the small spikes in the wings of the main stem. These fine structures can best be resolved in the model flow and one discovers (Fig. 14) both complete and truncated stems which correspond now to an exact collision with or passing nearby the *rear* stagnation point.

Furthermore, one can read off these pictures that the sequence of complete stems converges to the left boundary of the cluster according to a geometrical progression. The origin of this fact can be understood by taking trajectories from the inside of stems in this sequence. In this sequence, a few members of which are shown in Fig. 15, trajectories remain close to the figure eight orbit before reaching the wall. Two consecutive members of the sequence differ by performing an additional half revolution around this orbit of period one. In order to perform an additional half revolution, the distance of the initial conditions from the stable manifold of this periodic orbit must be smaller by a factor which is the square root of its stability exponent. Extracting the scal-

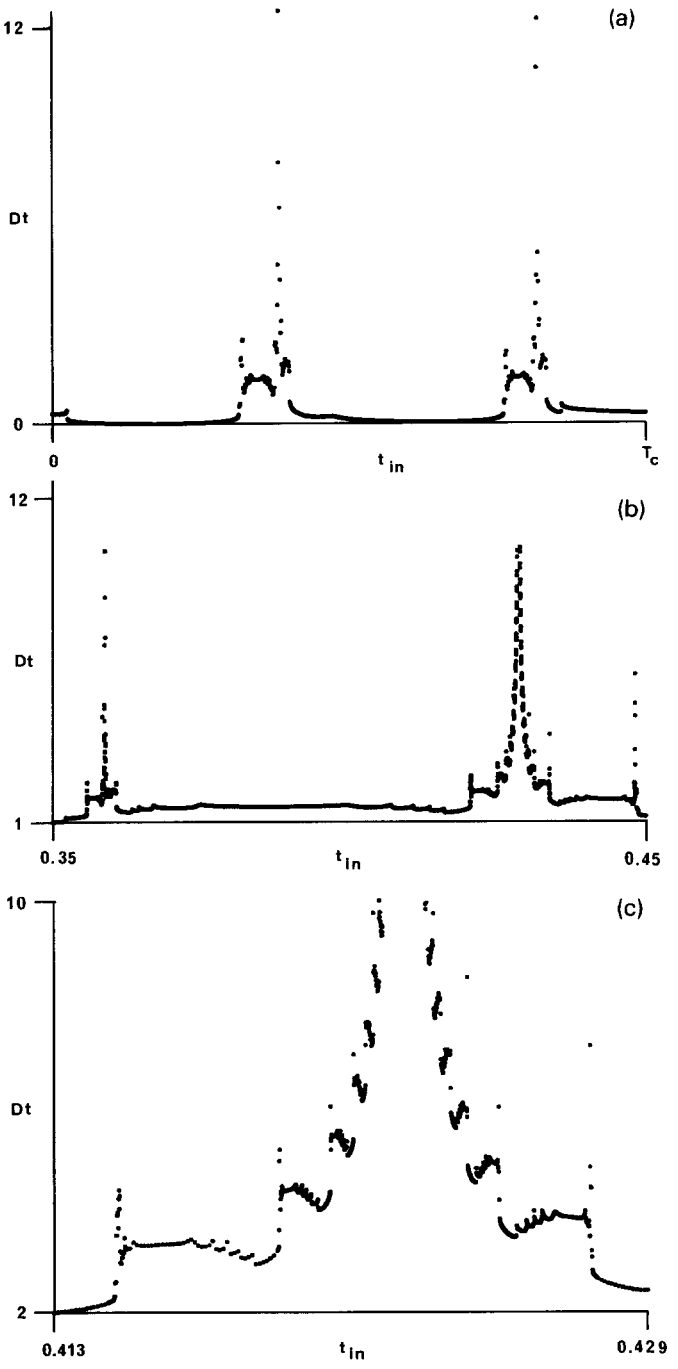

Fig. 13. Plot of the time delay function $Dt(t_{in})$ for $y_{in} = 0.0995$ based on Navier-Stokes data. (a) shows this function on its whole domain. (b) is a magnification of one of the small intervals containing singularities. (c) shows a further magnification.

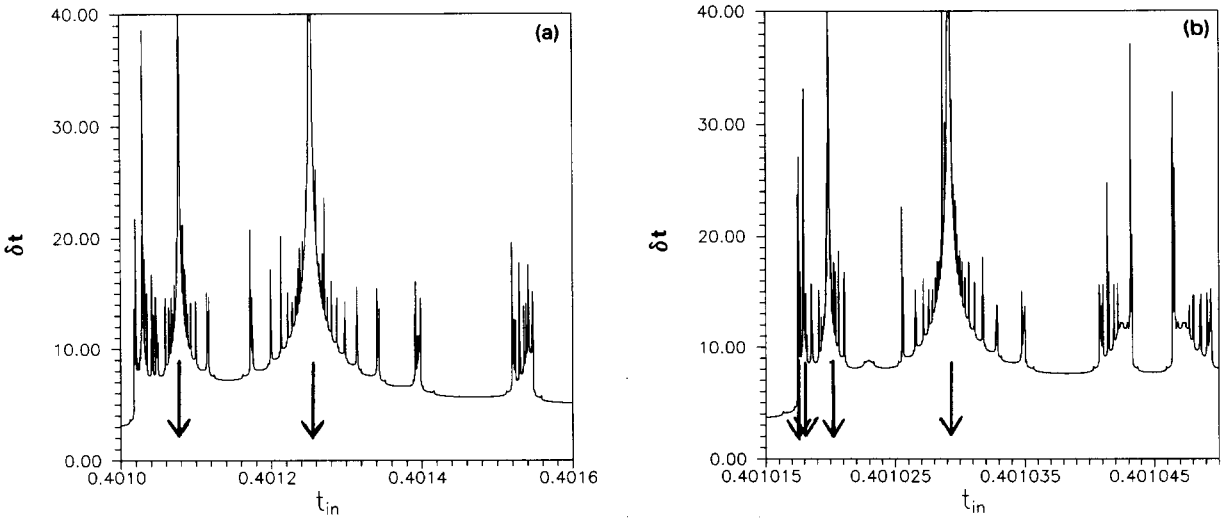

Fig. 14. Magnification of the time delay function on a very fine scale. This plot is based on the flow of the analytical model, for details see [27]. The arrows mark points around the centers of the stems and approach the left boundary of the cluster of singularities in a geometrical progression.

ing factors of the self-similiar structures in the time delay function provides thus a possibility for finding the local Lyapunov exponents of periodic orbits embedded into the chaotic set.

9. Conclusions

In this concluding section we give, based on the observations made in the paper, a brief summary of quantities that might be measured experimentally.

- Particle trajectories of complicated form can be observed, and simple periodic orbits or parts of them can be identified by means of trajectories shadowed by such periodic orbits.
- Streaklines converging in the wake of the obstacle to the unstable manifold of the chaotic set can be followed. The fractal dimension of the cross-section can be determined (e.g. by the method of [15]) which in case of an intermediate resolution should correspond to that of the hyperbolic component.
- Time delay statistics can be measured (similarly as it was done in a closed system [69]) and should be dominated by an algebraic decay with an exponent -2. (If the tangential velocity in the boundary layer decayed as the $(\beta-1)$st power of the distance, then this exponent would be $\beta/(1-\beta)$.) With initial conditions avoiding a direct collision with the cylinder wall, a short time exponential behaviour can be seen the decay of which defines the escape rate from the hyperbolic part of the chaotic set.
- From the dynamics of line segments the topological entropy of the chaotic set can be extracted.
- An alternative way of determining the escape rate is based on the streakline dynamics, from which an average Lyapunov exponent can be extracted, too.
- By means of ensemble methods also the chaotic set and its stable manifold could be visualized.
- The most difficult task could eventually be the measurement of the time delay function. On the crudest scale it should be dominated by stems that exhibit global algebraic behaviour. With fine resolution also self similar structures could be seen, the scaling properties of which provide information on the instability of the

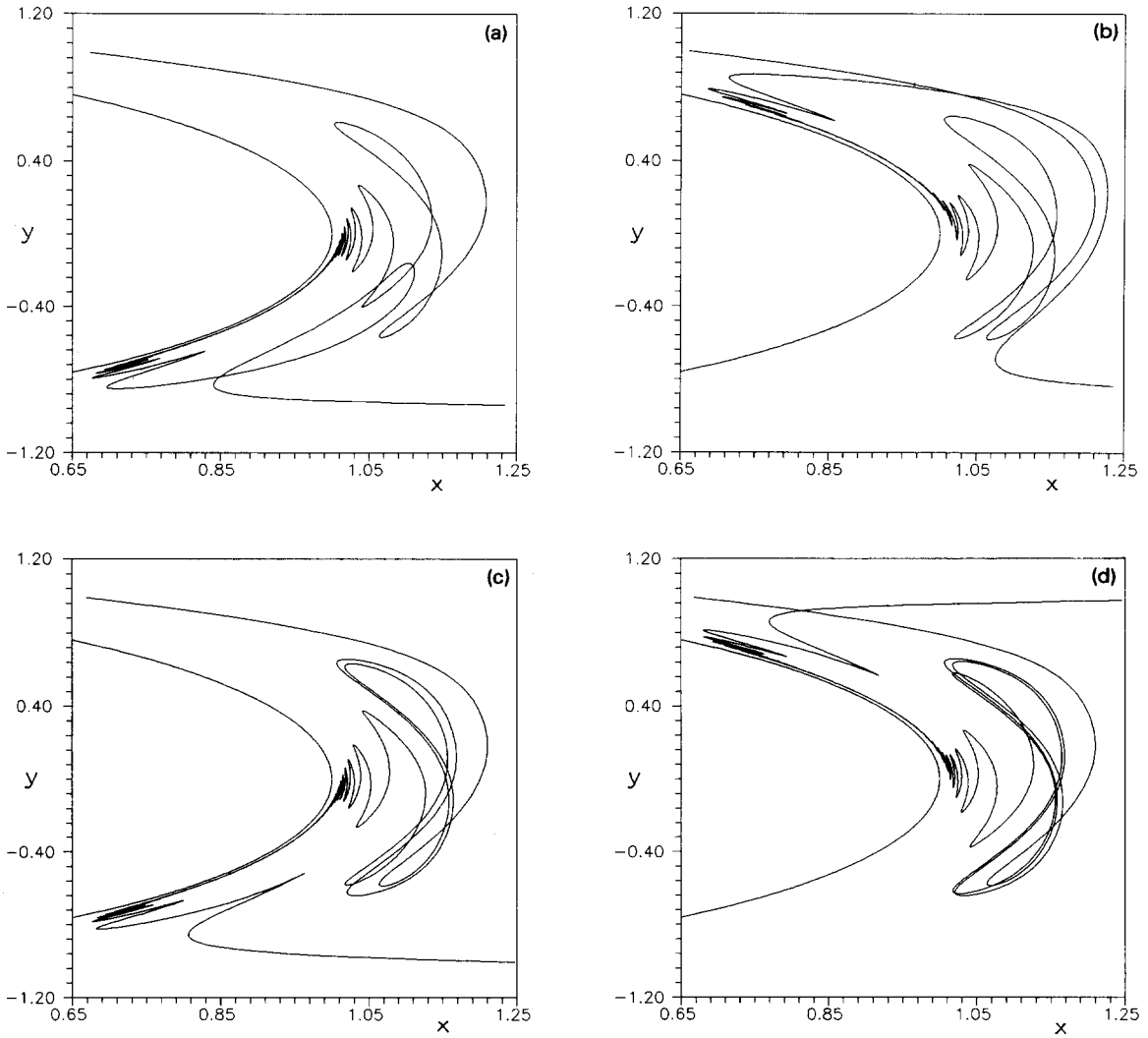

Fig. 15. A sequence of scattering trajectories corresponding to a sequence of stems seen in the time delay function of Fig. 14. The initial condition in Fig. 15a and b correspond to the arrows in Fig. 14a. Those of Fig. 15c and d correspond to the two middle arrows of Fig. 14b. For better visualization, different scales has been used on the axes.

shortest hyperbolic periodic orbits.

In the bulk of the paper we have treated incompressible flows in a 2-dimensional position space which lead to the analogy with Hamiltonian dynamics. This analogy was not essential for many concepts presented, e.g. for the time delay function and its statistics, for the existence of periodic orbits and their manifolds, for the invariant set and for the creation of streaklines. Therefore, the basic ideas of this paper work equally well also for 3-dimensional flows and for fluids with some compressibility.

Open systems provide an essential advantage over closed systems for the visualisation of the fractal phase space structures typical for chaotic dynamics. Because of the Poincaré recurrence in closed Hamiltonian systems, each point of the phase space belongs to a component of the invariant set. Therefore, the invariant set is not a fractal subset of the phase space. In a closed

system also the manifolds of periodic orbits are dense in a subset of nonzero measure and, accordingly, the long time limit of the streaklines do the same. They do not have empty gaps on all scales as typical for fractal patterns. In contrast, for open systems at least the component of the invariant set accessible by scattering trajectories is a fractal set of measure zero, and has gaps on all scales. The invariant manifolds are then fractals, too. Therefore, *only in open systems* does the distribution of advected particles converge towards a fractal pattern in the long time limit.

Realistic scattering experiments are performed in systems of mesoscopic or microscopic size where the semiclassical or wave properties are essential and lead to interference effects. Passive advection in the wake of an obstacle is, however, a pure classical phenomenon, and we think that it could thus be a promising candidate for investigating scattering chaos in a laboratory.

Acknowledgements

One of the authors (C.J.) thanks the Deutsche Forschungsgemeinschaft for financial support in form of a Heisenberg stipendium. This work has partially been supported by the Hungarian Research Foundation under the grant numbers OTKA 2090 and OTKA T4439 and by the Foundation for Higher Education and Research. The author (T.T.) is indebted to Prof. J.A. Yorke for a useful discussion, and to A. Péntek, K.G. Szabó and Z. Toroczkai for a critical reading of the manuscript. We thank Prof. S. Albeverio for his support for this work. The fluid dynamical computer program was constructed originally for the Priority Project " Finite Approximations in Fluid Dynamics " under the coordination of Prof. E. Krause. The Navier-Stokes flow computations have been done on the vector computer CDC-205 and the passive advection computations to it on the scalar computer CDC-992 of the Computer Center of the University Bochum. We thank the staff of the Computer Center and Dr. R. Mannshardt for their support.

Appendix A. The model flow

The analytic model used in the computations is defined by a streamfunction ψ. By choosing the center of the cylinder to lie in the origin, we write ψ in the following form:

$$\psi(x,y,t) = f(x,y)g(x,y,t) \tag{A.1}$$

The first factor

$$f(x,y) = 1 - \exp\{-a[(x^2+y^2)^{1/2} - 1]^2\} \tag{A.2}$$

yields the no-slip boundary condition at the cylinder's surface. The cylinder radius has been taken to be unity which can always be done by suitable rescaling the length scales. The coefficient $a^{-1/2}$ plays the role of the width of the boundary layer. This form of the streamfunction ensures that the tangential velocity tends linearly to zero as expected in a boundary layer. We use the boundary layer thickness as a free input parameter. A more realistic parameter could be used as well, e.g. taken from experiments. The radial component of the velocity vanishes quadratically which shows that the cylinder surface can be viewed as the union of an infinite number of degenerate parabolic fixed points.

The factor g contains the contributions of the vortices and of the background flow u_0. It reads

$$\begin{aligned} g(x,y,t) = &-wh_1(t)\, g_1(x,y,t) \\ &+wh_2(t)\, g_2(x,y,t) \\ &+u_0 ys(x,y) \end{aligned} \tag{A.3}$$

The first two terms describe the alternating birth, evolution and damping out of vortices 1 and 2 of equal strength but opposite sign. The quantities w and $h_i(t)$ stand for the overall vortex strength and amplitudes, respectively. Because of the alternating character, one has $h_2(t) =$

$h_1(t - T_c/2)$ where T_c denotes the time period of the flow. As a simple choice we took

$$h_1(t) = |\sin(\pi t/T_c)|. \tag{A.4}$$

The vortex centers are assumed to move parallel to the x-axis and with a constant velocity. Their x-coordinates are expected to change with time as

$$x_1(t) = 1 + L[(t/T_c) \bmod 1], \tag{A.5}$$

$$x_2(t) = x_1(t - T_c/2), \tag{A.6}$$

while the y-coordinates are constants,

$$y_1(t) = -y_2(t) \equiv y_0. \tag{A.7}$$

Both vortices pass a distance L during time T_c and then shed. These formulas describe a situation when vortex 1 is created at $(x = 1, y = y_0)$ at time zero when vortex 2 is just in its most developed state at $(x = 1 + L/2, y = y_0)$. Let α denote a characteristic ratio telling us how much longer the linear size of the vortices along the x-axis is than along the y axis. The contribution to the stream function of the vortices can then be expressed by the form

$$g_i(x,y,t) = \exp\left(-R_0\{[x - x_i(t)]^2 + \alpha^2[y - y_i(t)]^2\}\right) \tag{A.8}$$

where $R_0^{-1/2}$ is the characteristic linear size of the vortices. Note that the vortex stream functions are chosen to be Gaussians of finite amplitude in contrast to the singular form used e.g. in the theory of point vortices.

The last term in Eq. (A.3) gives the contribution to the stream function from the background flow of uniform velocity u_0. The factor

$$s(x,y) = 1 - \exp[-(x-1)^2/\alpha^2 - y^2] \tag{A.9}$$

is introduced in order to simulate in a phenomenological manner the shielding of the background flow just behind the cylinder. This is taken here into account by using the same elongation factor α as in case of the vortices.

In the analytical model no channel walls are incorporated because the most essential features of the advection process are connected with the boundary condition on the surface of the cylinder only. The form given above is sufficient to incorporate useful features of the Navier-Stokes flow. For streamlines of the model see [27].

In contrast to a solution of the Navier-Stokes equations which depends only on the Reynolds number and on the aspect ratio, the model stream function contains several parameters. The numerical values of them have been chosen in such a way that one obtains a phenomenological fit to the known solution of the computer simulation of the Navier-Stokes problem. For the case of $Re = 250$ and aspect ratio $r = 0.25$ treated in the paper, the vortices had an elongation factor 2 and a size of about 1.6 times the cylinder radius, disappeared at about two cylinder radius past the cylinder. Consequently, we have $\alpha = 2, R_0 = 0.35, L = 2$. Furthermore, we chose $y_0 = 0.3$. Since the vortex velocity was about 7 times slower than the background velocity, one obtains $u_0 = 14/T_c$. The value of $w = 0.06\,T_c$ was an appropriate vortex strength as it provided a considerable recirculation in the wake of the cylinder just like in the Navier-Stokes case. The parameter a determines the width of the boundary layer which in the Navier-Stokes flow is obviously different from unity. This width has essential influence on the distance of the periodic orbits from the wall of the cylinder, in a most pronounced way for the figure eight orbit, and also on their eigenvalues. In order to see a large number of hierarchical levels with good numerical precision we need small cycle eigenvalues. Therefore, we took $a = 1$ leading to convenient eigenvalues. At this point we definitely deviate from parameters of the Navier-Stokes flow but the results do not depend essentially on the particular value of a and our choice was motivated just by numerical convenience. The smooth form of the shielding function (see Eq. (17)), which is much softer than the one appearing in the Navier-Stokes

flow, has been chosen for similar reasons.

References

[1] E.A. Novikov and Y.B. Sedov, Soviet Phys. JETP 48, (1978) 440; JETP Lett. 29 (1979) 677.
[2] H. Aref, Ann. Rev. Fluid. Mech. 15 (1983) 345; J. Fluid. Mech. 143 (1984) 1.
[3] J. Chaiken, C.K. Chu, M. Tabor and Q.M. Tan, Phys. Fluids 30 (1987) 687.
[4] J.M. Ottino, The kinematics of mixing: stretching, chaos, and transport (Cambridge Univ. Press, Cambridge, 1989).
[5] H. Aref, Phil. Trans. R. Soc. London 333 (1990) 273.
[6] J.M. Ottino, Ann. Rev. Fluid. Mech. 22 (1990) 207.
[7] A. Provenzale, A.R. Osborne, A.D. Kirwan and L. Bergamasco, in: Nonlinear Topics in Ocean Physics, A.R. Osborne, ed. (Elsevier, Amsterdam, 1991).
[8] A. Crisanti, M. Falcioni, G. Paladin and A. Vulpiani, Riv. Nuov. Cim. 14 (1991) 1.
[9] F.J. Muzzio, P.D. Swanson and J.M. Ottino, Int. J. Bifurc. Chaos 2 (1992) 37.
[10] Y.T. Lau and J.M. Finn, Physica D 57 (1992) 283.
[11] K. Ouchi and H. Mori, Prog. Theor. Phys. 88 (1992) 467.
[12] A.A. Chernikov and G. Schmidt, Phys. Lett. A 169 51 (1992).
[13] L. Yu, E. Ott and Q. Chen, Phys. Rev. Lett. 65 (1990) 2935.
[14] L. Yu, E. Ott and Q. Chen, Physica D 53 (1991) 102.
[15] J.C. Sommerer and E. Ott, Science 259 (1992) 335.
[16] A.E. Perry, M.S. Chong and T.T. Lim, J. Fluid. Mech. 116 (1982) 77.
[17] R.J. Perkins and J.C.R. Hunt, in: Advances in Turbulence 2 (Springer, Berlin, 1989) pp. 286–91.
[18] R.W. Davis and E.F. Moore, J. Fluid. Mech. 116 (1982) 475.
[19] S. Jones and H. Aref, Phys. Fluids 31 (1988) 469.
[20] S. Jones, O. Thomas and H. Aref, J. Fluid. Mech. 209 (1989) 335.
[21] V. Rom-Kedar, A. Leonard and S. Wiggins, J. Fluid. Mech. 15 (1990) 345.
[22] K. Shariff, T.H. Pulliam and J.M. Ottino, Lect. Appl. Math. 28 (1991) 613.
[23] W.R. Young and S.W. Jones, Phys. Fluids A 3 (1991) 1087;
S.W. Jones and W.R. Young, Physica D 76 (1994) 55, these proceedings.
[24] C. Jung and E. Ziemniak, J. Phys. A 25 (1992) 3929.
[25] L. Tang, F. Wen, Y. Yang, C.T. Crowe, J.N. Chumg and T R. Troutt, Phys. Fluids A 4 (1992) 2244.
[26] K. Shariff and A. Leonard, Annu. Rev. Fluid. Mech. 24 (1992) 235.
[27] C. Jung, T. Tél and E. Ziemniak, Chaos 3 (1993) 555.
[28] J. Kadtke and E.A. Novikov, Chaos 3 (1993) 543.
[29] C. Jung and E. Ziemniak, in: IFIP Transactions, Fractals in the Natural and Applied Sciences, A41, M.M. Novak, ed. (Elsevier, Amsterdam, 1994) pp. 211–219.
[30] S. Bleher, C. Grebogi and E. Ott, Physica D 46 (1990) 87.
[31] U. Smilansky, in: Chaos and Quantum Physics, M.-J. Giannoni et al., eds. (Elsevier Science, New York, 1992).
[32] T. Tél, in: Directions in Chaos, vol. 3, Bai-lin Hao, ed. (World Scientific, Singapore, 1990) pp. 149–221.
[33] C. Jung, Acta. Phys. Polonica 23 (1992) 177.
[34] F.R. Hama, J. Aero. Sci. 24 (1957) 156.
[35] F. Homann, Forsch. Gebiet Ing 7 (1936) 1;
also in P. Plaschko, E. Berger and R. Peralta-Fabi, Phys. Fluids A 5 (1993) 1718.
[36] M. König, B.R. Noack and H. Eckelmann, Phys. Fluids A 5 (1993) 1846.
[37] F. Ohle and H. Eckelmann, Phys. Fluids A 4 (1992) 1707.
[38] G. Karniadakis and G. Triantafyllon, J. Fluid Mech. 238 (1992) 1.
[39] K.R. Sreenivasan, Ann. Rev. Fluid Mech. 23 (1991) 539.
[40] A. Kourta, H.C. Boisson, P. Chassaing and H. Ha Minh, J. Fluid Mech. 181 (1987) 141.
[41] H. Choi and P. Moin, Phys. Fluids A 2 (1990) 1450; M.J. Lee, J. Kim and P. Moin, J. Fluid Mech. 216 (1990) 561.
[42] J. Eggers and S. Grossmann, Phys. Fluids A 3 (1991) 1958.
[43] S. Albeverio and R. Hoegh-Krohn, Stoch. Proc. Appl. 31 (1989) 1; in: Proc. Confer. Les Embiez (1980).
[44] A. Crisanti, M. Falcioni, A. Provenzale, P. Tanga and A. Vulpiani, Phys. Fluids A 4 (1992) 1805.
[45] R. Mallier and M. Maxey, Phys. Fluids A 3 (1991) 1481.
[46] J.B. McLaughlin, Phys. Fluids 31 (1988) 2544.
[47] T. Tél, J. Phys. A. 22 (1989) L691.
[48] P. Cvitanović and B. Eckhardt, Phys. Rev. Lett. 63 (1989) 823.
[49] C. Jung and P. Richter, J. Phys. A. 23 (1990) 2847.
[50] Y.T. Lau, J.M. Finn and E. Ott, Phys. Rev. Lett. 66 (1991) 978.
[51] Y.C. Lai, T. Tél and C. Grebogi, Phys. Rev. E 48 (1993) 709.
[52] Z. Kovács and T. Tél, Phys. Rev. Lett. 64 (1990) 1617.
[53] T. Tél, Phys. Rev. A 44 (1991) 1034.
[54] F.H. Harlow and J.E. Welch, Phys. Fluids 8 (1965) 2182.
[55] B.E. Launder and T.H. Massey, J. Heat Transfer 100 (1978) 565.
[56] F. Varosi, C. Grebogi and J.A. Yorke, Phys. Lett. A 124 (1987) 59.
[57] M. Van Dyke, An Album of Fluid Motion (The Parabolic Press, Stanford, 1982).
[58] G.-H. Hsu, E. Ott and C. Grebogi, Phys. Lett. A 127 (1988) 199.

[59] S.W. McDonald, C. Grebogi, E. Ott and J. Yorke, Physica D 17 (1985) 125.
[60] S. Newhouse and T. Pignataro, J. Stat. Phys. 72 (1993) 1331.
[61] H. Kantz and P. Grassberger, Physica D 17 (1985) 75.
[62] B.R. Noack and H. Eckelmann, Physica D 56 (1992) 151.
[63] C.F. Karney, Physica D 8 (1983) 360.
[64] J.D. Meiss and E. Ott, Phys. Rev. Lett. 55 (1985) 2741.
[65] M. Ding, T. Bountis and E. Ott, Phys. Lett. A 151 (1990) 395.
[66] Y. Lai, R. Blümel, E. Ott and C. Grebogi, Phys. Rev. Lett. 68 (1992) 3491.
[67] Y. Lai, C. Grebogi, R. Blümel and M. Ding, Phys. Rev. A 45 (1992) 8284.
[68] C.F. Hillermeier, R. Blümel and U. Smilansky, Phys. Rev. A 45 (1992) 3486.
[69] T.H. Solomon, E.R. Weeks and H.L. Swinney, Phys. Rev. Lett. 71 (1993) 3975.
[70] B. Eckhardt and C. Jung, J. Phys. A 19 (1986) L829.
[71] R.J. Adrian, Annu. Rev. Fluid Mech. 23 (1991) 261.
[72] E.M. Ziemniak, N. Mitra and M. Fiebig, Notes on Numerical Fluid Mechanics, vol. 25, E.H. Hirschel, ed. (Vieweg, Braunschweig, 1989) p. 409.
[73] E.M. Ziemniak, N. Mitra and M. Fiebig, in: Numerical Methods in Laminar and Turbulent Flow, vol. 6, C. Taylor, P. Gresho, R. Sani and J. Hauser, eds. (Pineridge Press, Swansea, 1990) p. 553.
[74] E.M. Ziemniak, in: Numerical Methods in Laminar and Turbulent Flow, vol. 6, C. Taylor, P. Gresho, R. Sani and J. Hauser, eds. (Pineridge Press, Swansea, 1990) p. 543.